Advanced Physical Research
Vol.7, No.2, 2025, pp.171-183
https://doi.org/10.62476/apr.72171

# INFLUENCE OF $Bi_4Ti_3O_{12}$ DOPING ON STRUCTURE, MICROSTRUCTURE, AND ELECTRICAL PROPERTIES OF (K,Na,Li)(Nb,Sb)$O_3$ CERAMICS

**Le Dai Vuong**[1,*], **Nguyen Dang Nhat**[1], **Vo Quang Nha**[1], **Huynh Thi Thuy Linh**[1], **Phan Tuan Anh**[2], **Vo Thi Thanh Kieu**[2]

[1]School of Engineering and Technology - Hue University, Hue City, Vietnam
[2]Hue Industrial College, Hue City, Vietnam

**Abstract.** This study used a molten salt method to fabricate the templates of $Bi_4Ti_3O_{12}$ (BIT). The as-synthesized BIT templates exhibited orthorhombic perovskite structures with 5–20 $\mu m$ long and 0.5–1 $\mu m$ wide plate-like morphologies. The results showed that using BIT templates improved the piezoelectric properties of the $(1-x)(K_{0.48}Na_{0.48}Li_{0.04})(Nb_{0.95}Sb_{0.05})O_3 - xBi_4Ti_3O_{12}$ ceramics [$(1-x)$KNLNS – $x$BIT ceramics, $x$ = 0.0, 0.01, 0.02, and 0.03]. The experimental results revealed that the $(1-x)$KNLNS – $x$BIT samples sintered at 1100 °C had pure perovskite phases for a low BIT content ($x \leq 0.02$). The $(1-x)$KNLNS – $x$BIT sample sintered at 1100 °C showed good densification behaviors and a high density for a 0.02 mol BIT content. The 0.98KNLNS – 0.02BIT ceramics exhibited a high ceramic density of 4.51 g/cm$^3$, with a fairly uniform microstructure, clear grain boundaries, and a 1.29 $\mu m$ large grain size. Optimum piezoelectric properties of $k_p$ = 0.36, $d_{33}$ = 189 pC/N, $\varepsilon_r$ = 1017, $Q_m$ = 115, and a high Curie temperature $T_C$ = 381°C were obtained in 0.98KNLNS – 0.02BIT ceramics.

**Keywords**: Lead-free ceramics, KNLNS-BIT, $Bi_4Ti_3O_{12}$ templates, piezoelectric properties.
**Corresponding author:** L. Dai Vuong, School of Engineering and Technology - Hue University, Hue City, Vietnam, e-mail: *ldvuong@hueuni.edu.vn*
*Received: 21 April 2025; Revised: 22 May 2025; Accepted: 30 May 2025; Published: 24 June 2025.*

## 1 Introduction

Lead-free $(K_x,Na_{1-x})NbO_3$ ceramics (KNN ceramics), formed using ferroelectric $KNbO_3$ and antiferroelectric $NaNbO_3$, are promising replacements for the PZT-based ceramics and widely expand the applications of lead-free ceramics due to their outstanding electrical properties with excellent piezoelectric properties and a high Curie temperature ($T_C$ > 420°C) (Vuong et al., 2023; Tu et al., 2025).

However, synthesizing pure KNN ceramics and controlling the quality using a solid phase reaction method at high temperatures is often difficult due to the evaporation of the Na and K alkali metals. This is detrimental to the stability of the electrical properties of the KNN ceramics (Dong et al., 2017; Tu et al., 2024a). Therefore, KNN ceramics are studied and improved using different impurities, such as Sb or Ti in place of Nb, and Li and Bi in place of Na and K, or modified fabrication through two-step sintering (Vuong et al., 2023; Dong et al., 2017; Vuong et al., 2025).

The enhanced performance of KNN ceramics has been attributed to the formation of a polymorphic phase transition (PPT) through multi-element doping (e.g., Sb, Bi, Li, Ti, Sr, Ba), analogous to the morphotropic phase boundary observed in PZT-based ceramics (Tu &

Tho, 2023). Zhao *et al.* suggested that adding Li, Sb, and Ta into the KNN structure could establish the PPT of (Na,K,Li)(Nb,Ta,Sb)$O_3$ ceramics, which enhanced the stability of ceramics to improve the piezoelectric properties Zhao et al. (2014). Similarly, Li *et al.* reported that Li, Ta, Sb co-doped (K,Na)$NbO_3$ ceramics obtained excellent piezoelectric properties with the piezoelectric constant $d_{33}$ = 280 pC/N, dielectric constant $\varepsilon_r$ = 1775, and $P_r$ = 18.8 $\mu$C/cm$^2$ when the Li, Ta, and Sb contents were 0.0375, 0.06, and 0.07 mol, respectively (Li et al., 2015).

In a previous study by the author of this study, ($K_{0.48}Na_{0.48}Li_{0.04}$)($Nb_{0.95}Sb_{0.05}$)$O_3$ (KNLNS) ceramics synthesized using two-step sintering obtained good piezoelectric parameters, with the electromechanical coupling factor $k_p$ = 0.33, $d_{33}$ = 195 pC/N, and $P_r$ = 16.1 $\mu$C/cm$^2$ (Vuong et al., 2023).

Additionally, an earlier study by this author showed that adding 0.15 mol of $Bi_4Ti_3O_{12}$ (BIT) into $Bi_{0.5}(Na_{0.4}K_{0.1})TiO_3$ ceramics could improve the electrical properties to achieve expected values of $\rho$ = 6.19 g/cm$^3$, $P_r$ = 16 $\mu$C/cm$^2$, $\varepsilon_r$ = 1323, dielectric loss (tan$\delta$) = 0.045, and energy-storage density of 0.12 J/cm$^3$ at 46.3 kV/cm.

Dong et al. (2017) reported that ($K_{0.4425}Na_{0.52}Li_{0.0375}$)($Nb_{0.87}Ta_{0.06}Sb_{0.07}$)$O_3$ ceramics doped with 0.50 mol% BIT exhibited relatively high piezoelectric properties of $d_{33}$ = 255 pC/N, $k_p$ = 0.451, and mechanical quality factor $Q_m$ = 186 (Dong et al., 2017).

BIT is one of the simplest bismuth titanate compounds, with a perovskite structure composed of alternating layers of $Bi_2O_3$ and $TiO_2$ (Wang et al., 2013). The plate-like morphologies of BIT are beneficial for synthesizing oriented KNN-based ceramics (Tu et al., 2024a). This study synthesized BIT templates and examined the influence of BIT doping on the structure, microstructure, and electrical properties of the (K, Na, Li)(Nb, Sb)$O_3$ ceramics.

## 2 Experimental

The starting materials, including $Bi_2O_3$ (99.5%) and $TiO_2$ (99.5%), were weighed and milled in ethanol for 10 h using a planetary ball mill. Subsequently, the as-prepared powders were dried at 200 °C for 3 h and calcined at 600 °C for 2 h to obtain the amorphous BIT precursor powder. Subsequently, the BIT powder was mixed in molten NaCl salt and sintered at 1050 °C for 2 h (Fig. 1(a)). The formation of BIT templates is represented in Equation (Tu & Vuong, 2024b).

$$2Bi_2O_3 + 3TiO_2 \rightarrow Bi_4Ti_3O_{12} + \frac{1}{2}O_2 \tag{1}$$

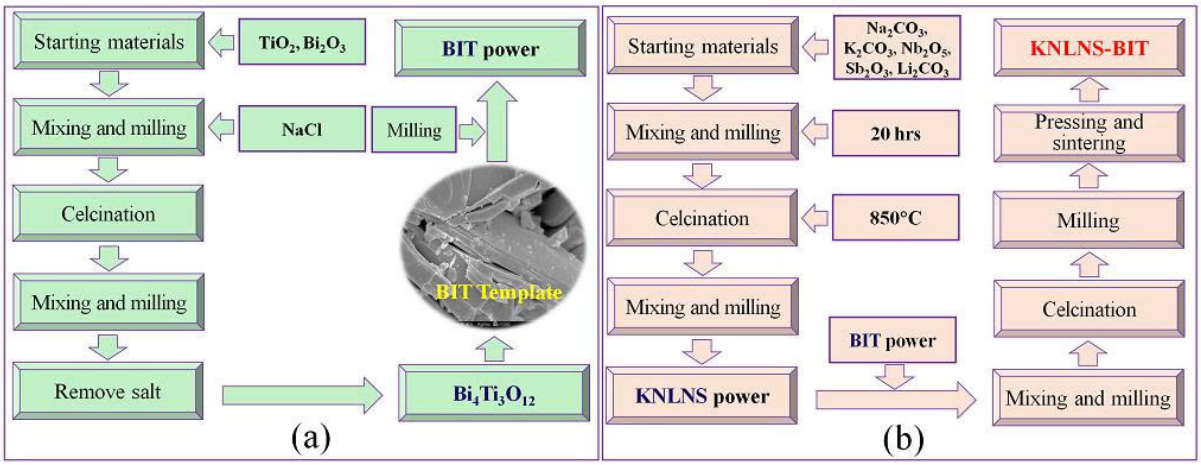


**Figure 1:** Synthesis process of BIT templates (a); and KNLNS–BIT ceramics (b).

The KNLNS-based powder was fabricated using a conventional solid-state reaction method. The starting materials in this stage included $Na_2CO_3$, $K_2CO_3$, $Nb_2O_5$, $Sb_2O_3$, and $Li_2CO_3$,

which were milled for 20 h using a planetary ball mill in an ethanol environment (Fig. 1(b)). Subsequently, this mixture was dried and calcined at 850 °C for 2 h to form the KNLNS compound.

Subsequently, KNLNS and BIT powders were weighed according to the ceramic formula of

$$(1-x)(K_{0.48}Na_{0.48}Li_{0.04})(Nb_{0.95}Sb_{0.05})O_3\text{–}xBi_4Ti_3O_{12}$$

$$[(1-x)KNLNS\text{–}xBIT, x = 0.0, 0.01, 0.02, 0.03],$$

followed by 10 h of milling and 2 h of re-calcining at 850 °C to form the BIT-doped KNLNS compound (Fig. 1(b)). Subsequently, the BIT-doped KNLNS compound was re-milled for 20 h, followed by pressing into 1.5 mm thick disks with 12 mm diameter under 1.5 T/cm$^2$ and sintering at 1150 °C to form BIT-doped KNLNS ceramics.

The crystal structures and surface morphologies of the $(1-x)$KNLNS – $x$BIT ($x = 0.0$, 0.01, 0.02, 0.03) ceramic samples were examined using X-ray diffraction (XRD) and scanning electron microscopy (SEM), respectively. The density and ferroelectric properties of the ceramic samples were determined using the Archimedes method and the Sawyer–Tower method, respectively. The piezoelectric properties of the ceramic samples were measured by poling them in a silicone oil bath at 60 °C through the application of a 35 kV/cm electric field for 25 min.

# 3 Results and Discussion

## 3.1 Characteristics of the BIT Templates

The structures of the BIT templates sintered at 1050 °C for 2 h and the major findings of their XRD analysis within the $2\theta$ range of 10–60° are shown in Fig. 2(a). The as-synthesized BIT templates primarily exhibited orthorhombic perovskite structures.

As displayed in Fig. 2(a), the observed peaks at $2\theta$ angles of 10.78°, 16.18°, 21.65°, 23.27°, 26.89°, 30.05°, 32.75°, 36.85°, 38.39°, 39.73°, 42.85°, 47.27°, 51.47°, and 56.96°, respectively, corresponded to the (004), (006), (008), (111), (115), (117), (0012), (1111), (0014), (028), (0016), (2012), and (222) planes of $Bi_4Ti_3O_{12}$ Tu & Vuong (2024b), with the intensity of the (006), (008), and (0014) peaks corresponding to the $a$–$b$ plane perpendicular to the $c$-axis of the $Bi_4Ti_3O_{12}$ sample, which was compared with reported values of $Bi_4Ti_3O_{12}$ crystal Xie et al. (2022); Chen et al. (2016).

Furthermore, the SEM images of the BIT templates indicated that most grains were large and laminated, which is a primary characteristic of $Bi_4Ti_3O_{12}$. The BIT templates were composed of 5–10 $\mu$m long and 0.5–1 $\mu$m wide plate-like morphologies, as shown in Fig. 2(b). The microstructural images also reflected the orientation structural characteristics of the BIT templates with highly intensive (00$l$) diffraction peaks of (060), (080), and (0140), and the major (171) peak was severely reduced, as shown in Fig. 2(a), similar to the study reported by Long *et al.* Long et al. (2017). The energy-dispersive X-ray spectroscopy (EDS) spectrum of the BIT templates sintered at 1050 °C for 2 h is presented in Fig. 2(c). The homogeneous distribution of all elements was consistent with the theoretical design and included Bi, Ti, and O elements in the BIT templates, which indicated the successful synthesis of samples. The mass percentage of the Bi element was about 60.71 wt.%, and its energy value was localized at 2.42, 10.82, and 13.02 keV. The mass percentages of Ti and O elements were about 12.63 wt.% and 26.66 wt.%, respectively (Fig. 2(d)). Additionally, the energy values were localized at 4.97 and 0.53 keV for Ti and O, respectively (Fig. 2(d)). It is well known that the solid reaction between $Bi_2O_3$ and $TiO_2$ under the support of NaCl salt obtained the BIT nuclei. The nuclei aggregated and rearranged to form the BIT matrix with a plate-like shape, as shown in Fig. 2(b). The BIT structure consisted of alternating layers of pseudo perovskite blocks and fluorite-like bismuth oxygen layers with the $(Bi_2O_2)^{2+}$ composition. In this structure, the O–Ti–O chains along the c-axis were interrupted by the presence of the $(Bi_2O_2)^{2+}$ layers and the translation of the

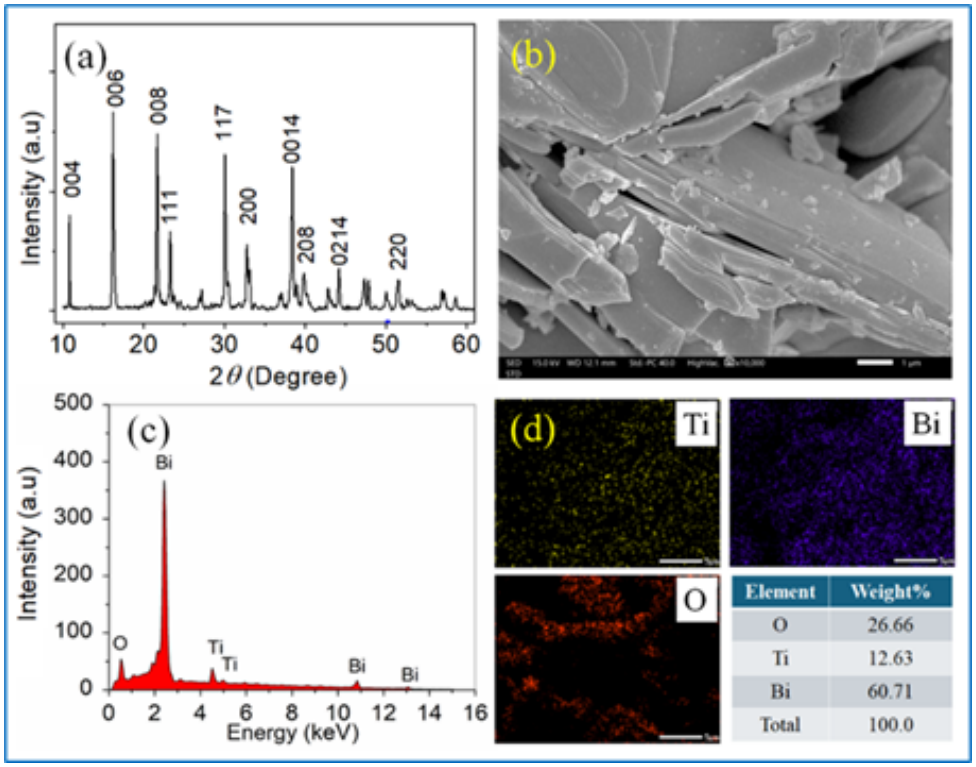


**Figure 2:** (a) XRD patterns; (b) SEM image; (c) EDS spectrum; and (d) element mappings of $Bi_4Ti_3O_{12}$ templates.

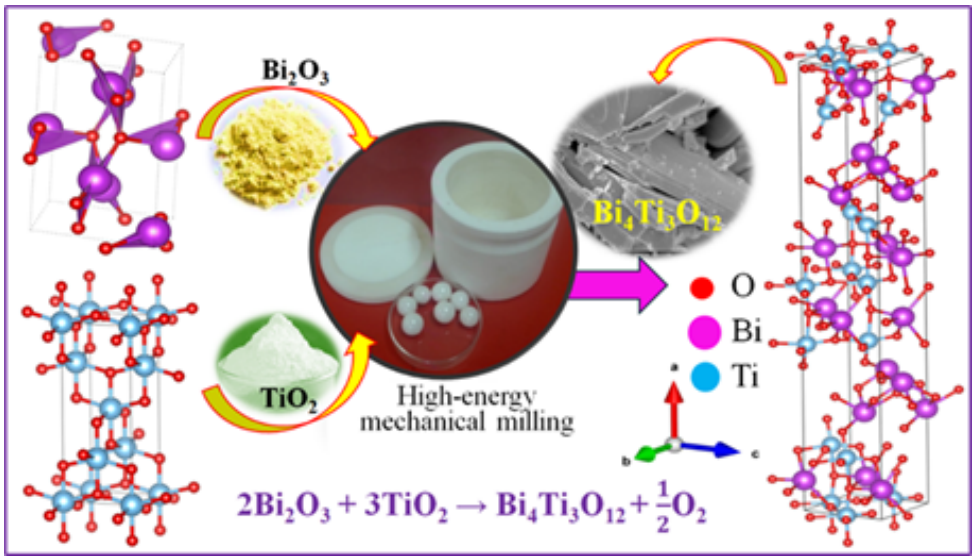


**Figure 3:** Formation mechanism of the BIT templates.

perovskite in the normal plane to the c-axis, as seen in Fig. 3. This structure originated the anisotropy of the physical properties, which could be easily adjusted parallel to the direction of crystal growth, suitable for synthesizing oriented ceramic systems and will be discussed in the next section.

The doping of BIT into the KNLNS ceramics is predicted to improve the microstructural orientation of the ceramics to enhance the electrical properties and increase the phase transition temperature $T_C$ due to the high $T_C$ characteristic ($T_C \approx 675\,^{\circ}\mathrm{C}$) suitable for power ultrasound applications Wendari & Ikhram (2022).

### 3.2 Characteristics of the BIT-doped KNLNS ceramics

The suitable sintering temperature was determined by sintering 0.99KNLNS–0.01BIT ceramics in the temperature range of 950–1100 °C, as shown in Fig. 4. Additionally, the bulk density and densification of KNLNS ceramics modified using different contents of BIT templates and sintering temperatures are shown in Fig. 4. As the sintering temperatures increased, the ceramic density and the relative density of the ceramics increased in the range of 3.81–4.51 g/cm$^3$ and 92.2–96.8%, respectively, as depicted in Fig. 4(a). The increase in the ceramic density was consistent with the shrinkage ratio and densification factor of the samples. In other words, at 1100 °C sintering temperature, the shrinkage ratio and the densification factor reached their highest values of 12.7% and 0.88, respectively (Fig. 4(b)).

These results were consistent with the results reported by Jiang et al. for the $K_{0.5}Na_{0.5}NbO_3$ ceramics, which were sintered at 1100 °C and had a bulk density of 4.39 g/cm$^3$ (relative density of 97.4%) Jiang et al. (2016). Dong et al. reported that the $(K_{0.4425}Na_{0.52}Li_{0.0375})(Nb_{0.87}Ta_{0.06}Sb_{0.07})O_3$ ceramics doped with 0.50 mol.% BIT exhibited the highest relativity density with a 1090 °C sintering temperature Dong et al. (2017).

It is well known that sintering temperatures effectively induce grain growth via the grain boundary migration. A good sintering temperature would contribute to increasing the shrinkage ratio and densification behaviors, improving the microstructure to increase the bulk density of the ceramics. In other words, the diffusion rate increases with the increased sintering temperature, improving the migration rate of grain boundaries and accelerating the grain growth process in ceramics Truong-Tho & Le Vuong (2021). As shown in Fig. 4(c), the bulk density of

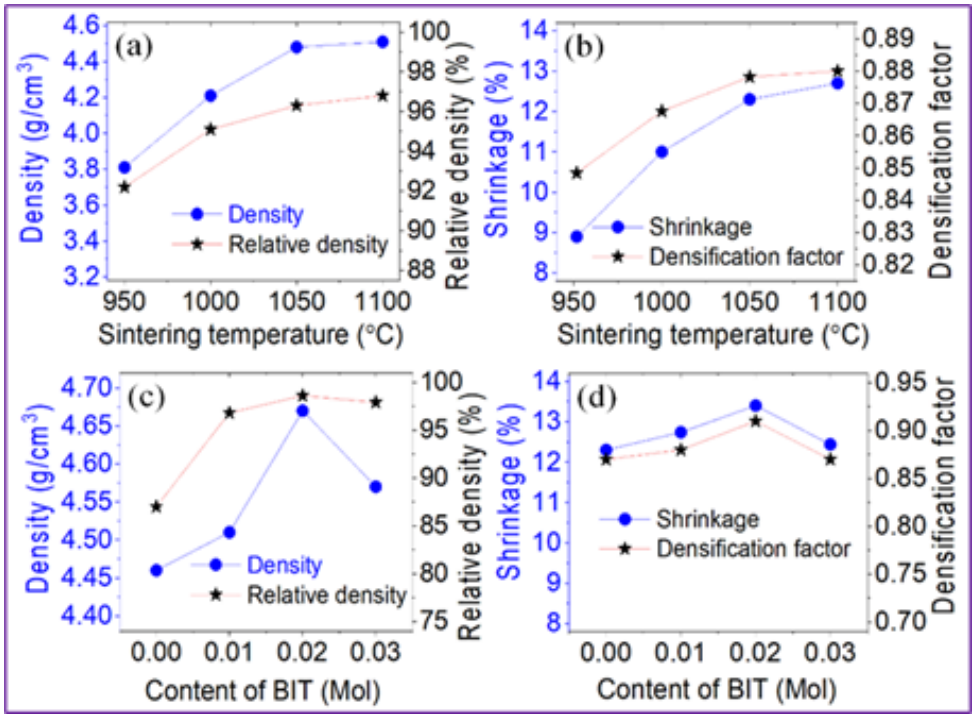


**Figure 4:** Density and densification of the $(1-x)$KNLNS-$x$BIT ($x$ = 0.0, 0.01, 0.02, and 0.03) ceramics as a function of sintering temperature.

the $(1-x)\text{KNLNS}-x\text{BIT}$ ($x$ = 0.0, 0.01, 0.02, and 0.03) ceramics depended on the BIT content in addition to the sintering temperature. The bulk density of the ceramics increased with the increased BIT content to reach the highest value at $x = 0.02$, followed by a further decrease. The BIT-doped KNLNS ceramics had a higher density than the undoped KNLNS ceramic because of the high density of BIT (theoretical density of 8.04 g/cm$^3$). Therefore, the BIT impurities contributed to increasing the ceramic density of the BIT-doped KNLNS ceramics.

It is well known that the BIT structure typically formed a liquid phase at 865−870°C, and the increased BIT doping content in the KNLNS ceramics increased the shrinkage ratio and densification behaviors (Fig. 4(d)). However, the shrinkage ratio and densification decreased for BIT contents exceeding 0.02 mol due to the solubility limits of Bi and Ti ions in the KNLNS lattice. Furthermore, the bulk density of ceramics depended on the microstructural characteristics of the ceramic, i.e., the degree of arrangement of the grains and grain boundaries.

The microstructure images of the 0.99KNLNS−0.01BIT ceramic sintered at different temperatures of 950, 1000, 1050, and 1100°C for 3 h are depicted in Fig. 5. The sintering temperature strongly influenced the microstructures of the BIT-doped KNLNS ceramics. For low sintering temperatures ($T_s < 1050$°C), the microstructures of the ceramics had many pores, and KNLNS-based particles were arranged loosely next to the BIT templates with rod-like structures. However, the number of pores sharply decreased with the increased sintering temperature, and the particles were tightly packed at the 1100°C sintering temperature, with the largest density and ceramic particle size of 4.45 g/cm$^3$ and 0.94 $\mu$m, respectively, as shown in Fig. 5(d). This phenomenon was because the ceramic density increased with the sintering temperature,

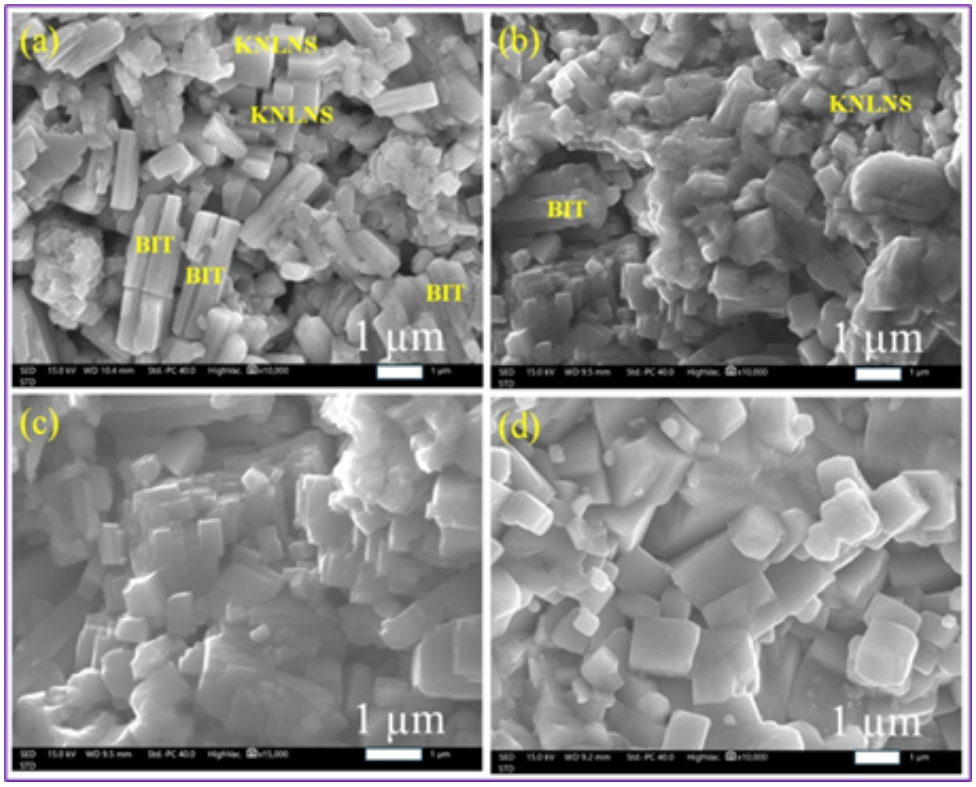


**Figure 5:** Microstructures of 0.99KNLNS–0.01BIT ceramics recorded at different sintering temperatures: (a) $950^0C$, (b) $1000^0C$, (c) $1100^0C$, and (d) $1100^0C$

which was related to the chemical reaction properties and the formation of oxygen vacancies that were beneficial for material transport during ceramic sintering Ullah et al. (2010). The ceramic growth mechanism was believed to follow the gradual grain growth mechanism, which meant crystal growth seeds from the BIT templates so that the KNLNS matrix particles grew according to the orientation of the original BIT templates, similar to the view of Wei *et al.* Wei et al. (2015).

Furthermore, the variation in the ceramic grain size with the sintering temperature is shown in Fig. 6. Initially, the ceramic grain size slightly decreased in the 950−1050°C temperature range. However, the grain size reached a maximum value of 0.94 $\mu$m at a sintering temperature of 1100°C. Additionally, the ceramics sintered at 1100°C showed a dense microstructure and a clear grain boundary, which provided enough energy to improve the migration rate of grain boundaries

and accelerate the grain growth process in the KNN-based ceramics under the support of liquid Bi phase due to the increase in the grain size Vuong & Tho (2017).

The microstructures of the $(1-x)$KNLNS $- x$BIT ($x = 0.0,\ 0.01,\ 0.02,$ and $0.03$) ceramics are shown in the SEM images in Fig. 7. Most grains of the ceramics had rectangular shapes with fairly uniform microstructures and clear grain boundaries. The grain size increased as the BIT content increased, reaching a maximum value of about 1.29 $\mu$m at $x = 0.02$, followed by a decrease (Fig. 8). The small grain size with many voids in the undoped KNLNS ceramic sample ($x = 0.0$) demonstrated its low ceramic density (Fig. 6). However, the microstructure of the ceramic became denser, the grains were more uniform, and the voids decreased with increasing BIT content, resulting in increased ceramic density, as discussed in Fig. 4.

It is evident from Fig. 7 that the addition of BIT increased the compactness and uniformity of grains due to the dissolution of $Bi^{3+}$ and $Ti^{4+}$ present in BIT into the KNLNS crystal lattice. Due to their similar radii, $Ti^{4+}$ ions (0.605 Å) penetrated the KNLNS crystal lattice and replaced the $Nb^{5+}$ (0.64 Å) and $Sb^{5+}$ (0.62 Å) ions, while the $Bi^{3+}$ ions (1.03 Å) replaced the $K^+$ (1.38 Å) or $Na^+$ (1.32 Å) ions, similar to the results reported by Zhang *et al.* Zhang et al. (2018).

Dong *et al.* Dong et al. (2017) suggested that adding BIT improved the uniformity of the grain size because BIT effectively lowered the sintering temperature and restrained the volatilization of the K and Na elements. However, BIT doping should be adjusted reasonably, as reported by Li *et al.* Li et al. (2022), since the ceramic grain size decreased and the number of pores increased when the BIT content exceeded 0.02 mol, which was attributed to the solubility limit of Ti and Bi ions in the matrix. The XRD patterns of the $(1-x)$KNLNS $- x$BIT

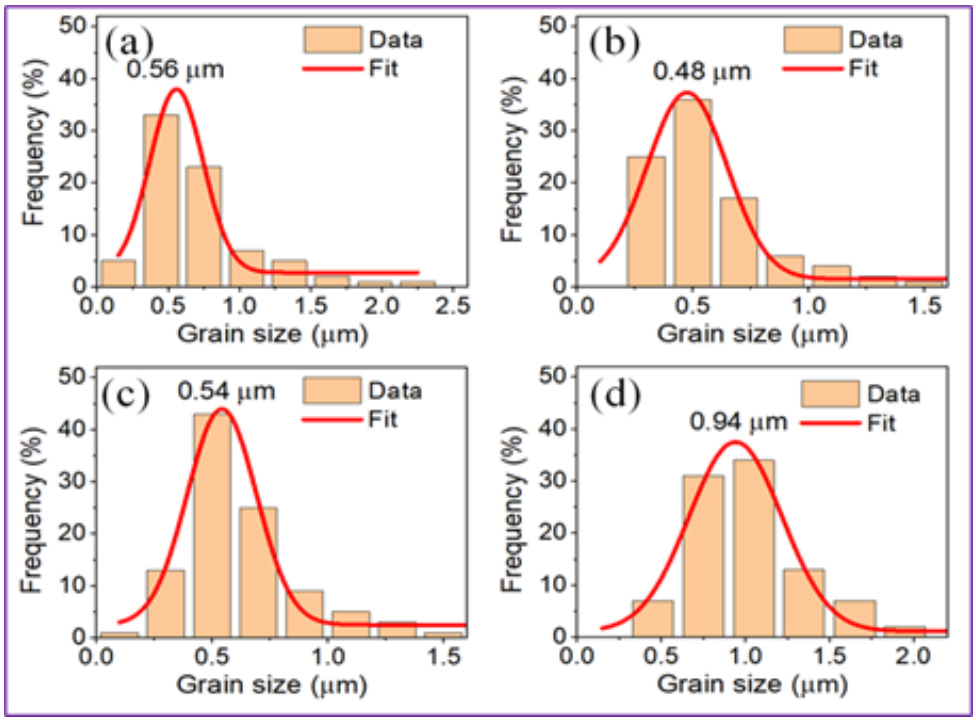


**Figure 6:** Grain size distribution of 0.99KNLNS–0.01BIT ceramic as a function of sintering temperature: (a) $950^0C$, (b) $1000^0C$, (c) $1100^0C$, and (d) $1100^0C$.

($x = 0.0$, 0.01, 0.02, and 0.03) ceramics sintered at 1100 °C are shown in Fig. 9. The XRD patterns were refined using Fullprof software to investigate the effect of $Bi_4Ti_3O_{12}$ templates on the phase structure of $(K_{0.48}Na_{0.48}Li_{0.04})(Nb_{0.95}Sb_{0.05})O_3$ ceramics. The samples had pure perovskite structures with no secondary phases at low BIT contents ($x \leq 0.02$ mol). However, secondary phase peaks appeared for a high $x$ value of 0.03 mol. Dong et al. reported similar XRD patterns for the $(1-x)(K_{0.4425}Na_{0.52}Li_{0.0375})(Nb_{0.87}Ta_{0.06}Sb_{0.07})O_3 - xBi_4Ti_3O_{12}$ ceramic structures Dong et al. (2017). Notably, as shown in Fig. 9 for the $(1-x)$KNLNS $- x$BIT ($x =$

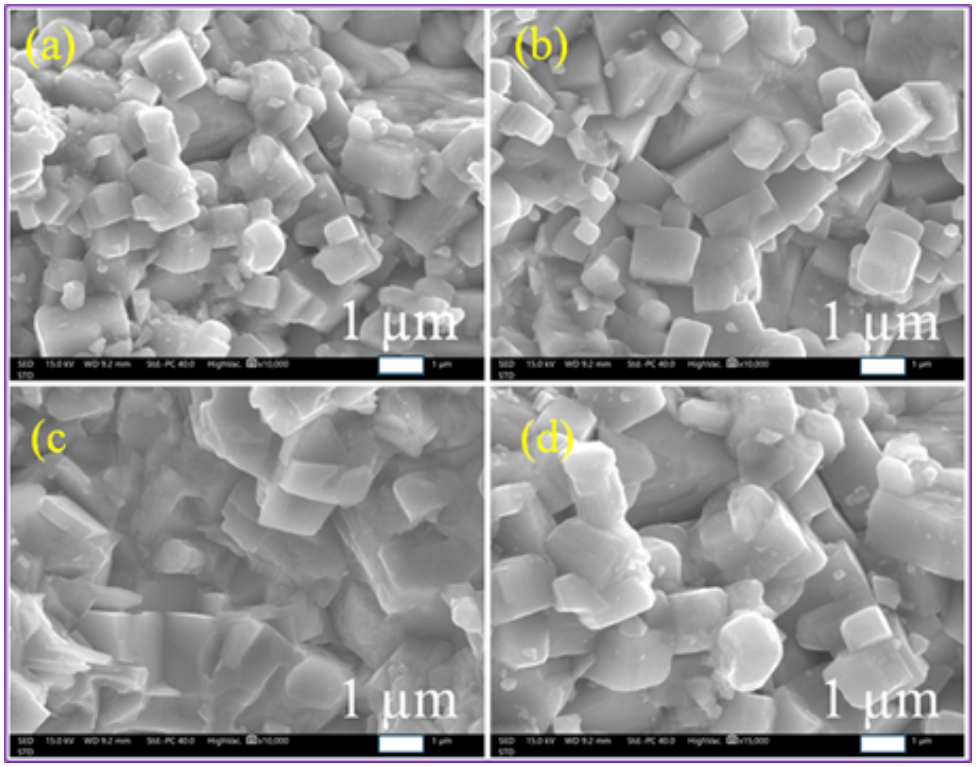


**Figure 7:** Microstructures of $(1-x)$KNLNS–$x$BIT ceramics recorded at different $x$: (a) $x = 0.0$, (b) $x = 0.01$, (c) $x = 0.02$, and (d) $x = 0.03$.

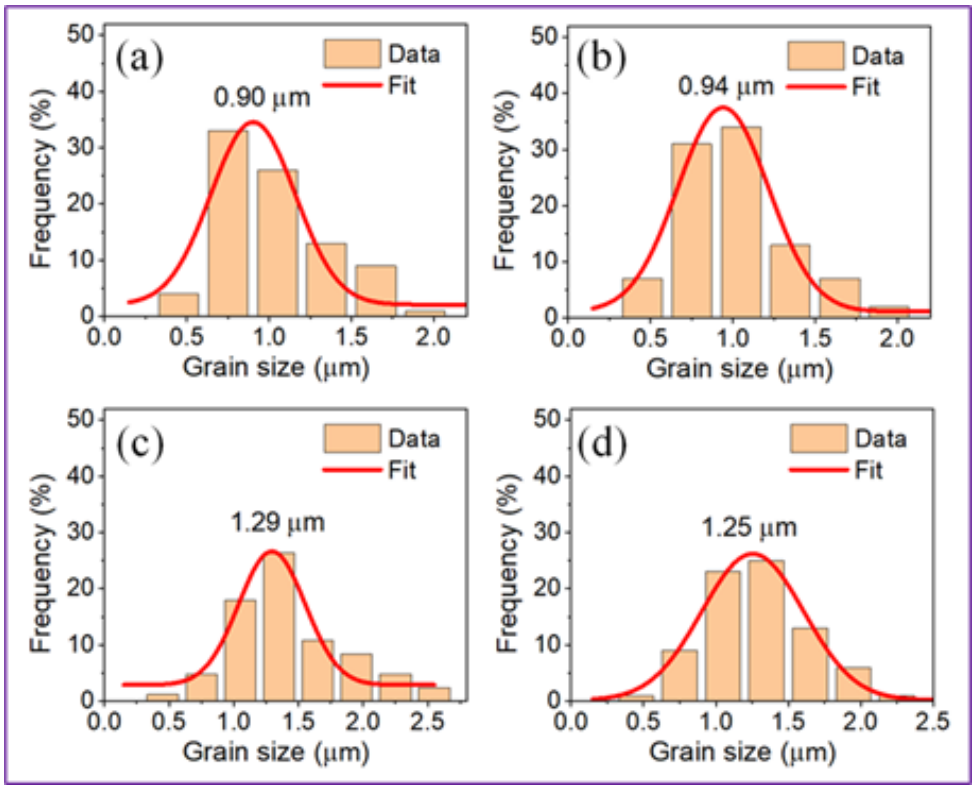


**Figure 8:** Grain size distribution of $(1-x)$KNLNS–$x$BIT ceramics recorded at different $x$: (a) $x = 0.0$, (b) $x = 0.01$, (c) $x = 0.02$, and (d) $x = 0.03$.

$0.0, 0.01, 0.02,$ and $0.03$) ceramics, pure KNLNS ceramic ($x = 0.0$) had an orthorhombic phase

(O-phase with space group = *Amm2*) with characteristic (022) and (200) peaks, similar to previous reports Tu et al. (2024a); Gio et al. (2021). As the BIT content further increased in the 0–0.01 range, the O-phase decreased and the rhombohedral $(200)_R$ phase (with space group = *R3m*) was enhanced. When $0.02 \leq x$, a rhombohedral $(200)_R$ phase was obtained, where the split peaks merged to become one peak, similar to the results reported by Dong et al. Dong et al. (2017). This phenomenon could be explained based on the difference in the radius of

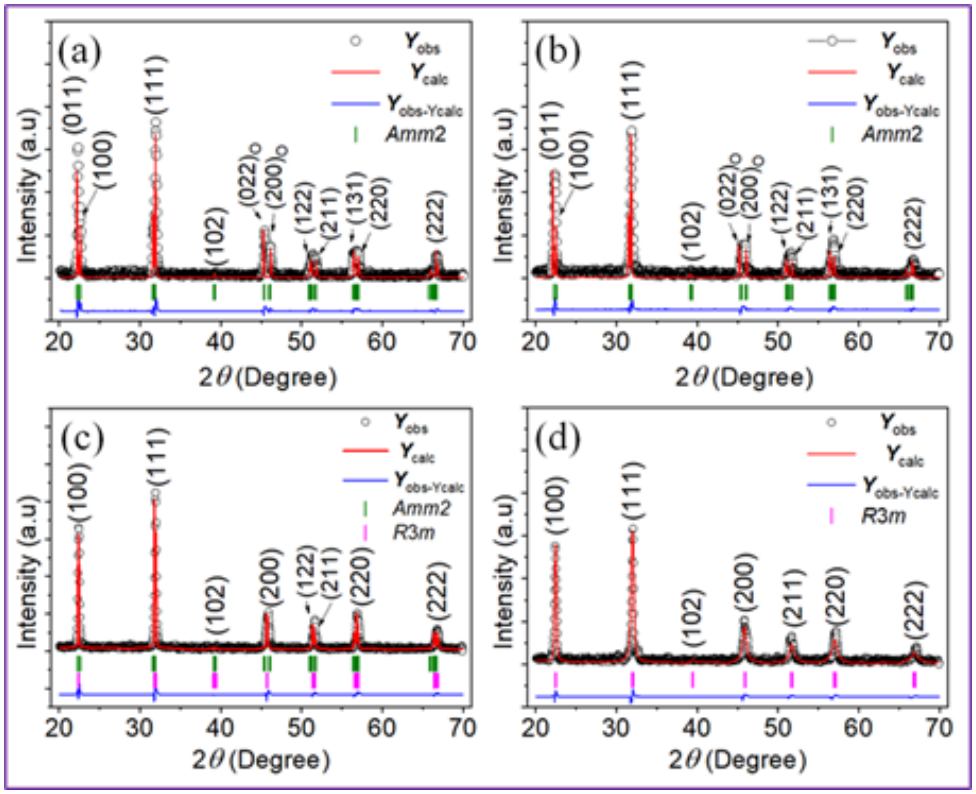


**Figure 9:** Rietveld refinement of XRD results of $(1-x)$KNLNS–$x$BIT ceramics with different $x$ contents: (a) $x = 0.0$, (b) $x = 0.01$, (c) $x = 0.02$, and (d) $x = 0.03$.

the ions. It was suggested that the $Ti^{4+}$ ions with a 0.605 Å radius could partially replace the $Nb^{5+}$ ions (0.64 Å) and $Sb^{5+}$ ions (0.62 Å). Meanwhile, the $Bi^{3+}$ ions with a 1.03 Å radius could partially replace the $K^+$ (1.38 Å) or $Na^+$ (1.32 Å) ions to form a uniform KNLNS–BIT structure. Moreover, this substitution would change the ceramic structure from the O-phase to the rhombohedral phase (R-phase) when the BIT content increased. In other words, using multiple doping could break the solubility limit of single doping and transform the O-phase to the R-phase in the $(1-x)$KNLNS $- x$BIT ($x = 0.0, 0.01, 0.02,$ and $0.03$) ceramics, which were predicted to exhibit good piezoelectric properties and are discussed in the following section. The variation of $\varepsilon$ and $\tan\delta$ with temperature in the 30–420 °C range for the $(1-x)$KNLNS $- x$BIT ($x = 0.0, 0.01, 0.02,$ and $0.03$) samples is shown in Fig. 10. As depicted in Fig. 10(a), the $\varepsilon(T)$ curves of the $(1-x)$KNLNS $- x$BIT ceramic samples had two obvious peaks: a peak at lower temperatures corresponding to the orthorhombic–tetragonal ferroelectric phase transition temperature ($T_{O-T}$) and the second peak at higher temperatures corresponding to $T_C$ Wang et al. (2021). The $T_{O-T}$ and $T_C$ phase transition temperatures of the ceramics were significantly influenced by the addition of BIT. Moreover, $T_C$ tended to increase as the BIT content increased, while $T_{O-T}$ followed an opposite trend. Specifically, the $T_{O-T}$ value decreased from 120 to $65^0C$ as the BIT content increased (from $x = 0.0$ to $x = 0.02$). In other words, the $T_{O-T}$ value for the 0.98KNLNS – 0.02BIT ceramics was $65^0C$. It is well known that raising $T_C$ was valuable for practical applications while lowering $T_{O-T}$ to near room temperature was beneficial for improving the electrical properties of the materials. Additionally, adding BIT to KNLNS

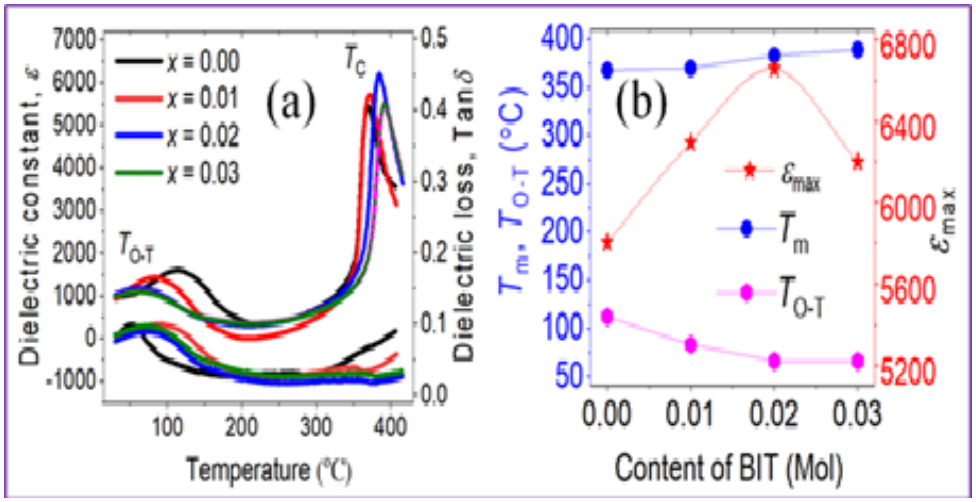


**Figure 10:** (a) The $\varepsilon$–$T$ curves of the $(1-x)$KNLNS–$x$BIT ceramics; (b) Values of $T_{\text{O-}T}$, $T_{\text{m}}$, and $\varepsilon_{\max}$ at different values of $x$.

ceramics could improve the dielectric properties and $T_C$ for the ceramics, as shown in Fig. 10(b). $T_C$ increased from 375 to 381 °C as the BIT content increased, which was explained by the high $T_C$ value of $\sim$ 675 °C for BIT and was similar to the results reported by Dong et al. Dong et al. (2017). As shown in Fig. 11(a), $\varepsilon_r$ and $\tan\delta$ depended on the BIT content measured at 1

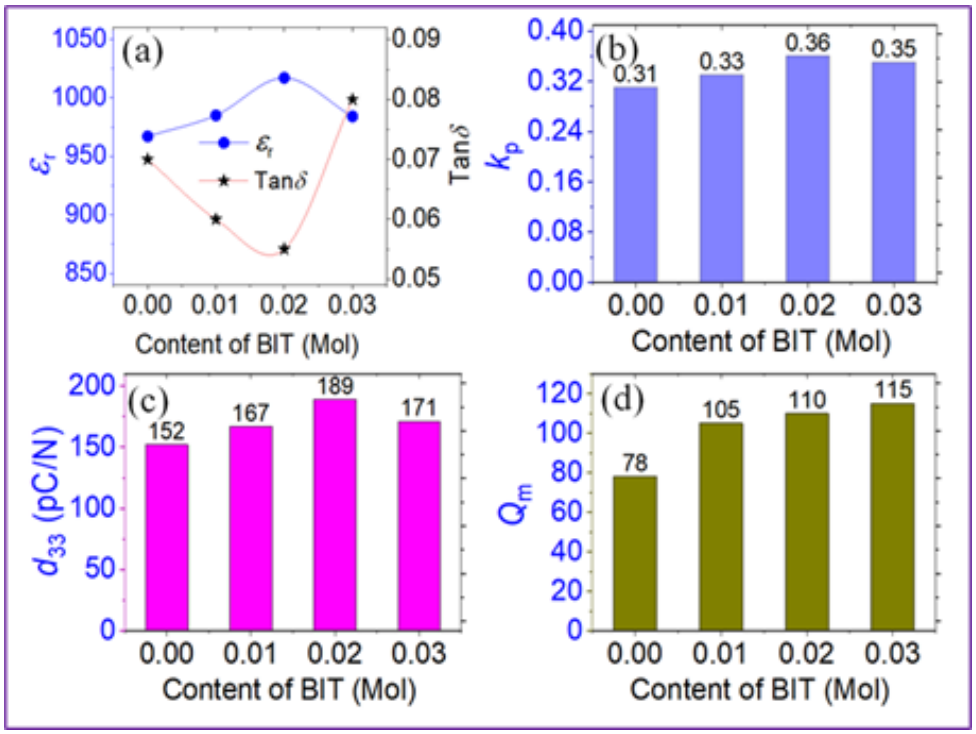


**Figure 11:** Piezoelectric dielectric parameters of $(1-x)$KNLNS–$x$BIT ceramics with different $x$ contents: (a) $\varepsilon_r$ and $\tan\delta$; (b) $k_p$; (c) $d_{33}$; and (d) $Q_m$.

kHz at $30^0C$. With the increased BIT content, $\varepsilon_r$ increased gradually to reach the maximum value of 1017 at $x = 0.02$. On the contrary, $\tan\delta$ gradually decreased with the increased BIT content to reach the minimum value of 0.055 at $x = 0.02$. Moreover, this was attributed to the increased grain size and the decreased number of grain boundaries, as shown in the SEM images in Fig. 7. Furthermore, the maximum dielectric constant ($\varepsilon_{\max}$) of the $(1-x)$KNLNS $-$ $x$BIT ($x = 0.0, 0.01, 0.02,$ and $0.03$) ceramics increased as the $x$ value increased to 0.02 to reach the

largest $\varepsilon_{\max}$ value of 6700, followed by a decrease in the $\varepsilon_{\max}$ value as $x$ further increased (Fig. 10(b)). The increase in the dielectric properties at $x = 0.02$ was thought to be due to the combining of the phase boundary and large particle size effects, where the domains had increased mobility, similar to the results reported by Tu et al. Tu & Tho (2023).

As shown in Fig. 11(b–c), the $k_p$ and $d_{33}$ values of the

$$(1-x)\text{KNLNS} - x\text{BIT}(x = 0.0, 0.01, 0.02, \text{and } 0.03)$$

ceramics changed as a function of $x$. The addition of BIT significantly affected the piezoelectric properties of the $(1-x)$KNLNS $- x$BIT ceramics. When the $x$ value increased from 0 to 0.03, the $k_p$ and $d_{33}$ values rapidly increased to reach the maximum values of 0.36 and 189 pC/N at $x = 0.02$, followed by a decrease. These results may be because the ceramics had a high density, large grain size, and increased orderly arrangement of the microstructures due to the optimized BIT content, which reduced the leakage current and enhanced the poling efficiency. Additionally, it is well-known that the formation of the phase boundary enhances the piezoelectric coefficient. The structure of the KNLNS ceramics changed from the O-phase to the R-phase due to the addition of BIT.

Furthermore, as mentioned earlier, the $Ti^{4+}$ ions with a 0.605 Å radius could partially replace the $Nb^{5+}$ (0.64 Å) and $Sb^{5+}$ (0.62 Å) ions, while the $Bi^{3+}$ ions with a 1.03 Å radius could partially replace the $K^+$ (1.38 Å) or $Na^+$ (1.32 Å) ions, which reduced the $T_{O-T}$ temperature to near room temperature (Fig. 10(a)) and improved the dielectric and piezoelectric properties of the ceramic, as reported by Refs. Tu & Tho (2023); Li et al. (2022).

An increase in the BIT content in the $(1-x)$KNLNS $- x$BIT ceramic samples linearly increased $Q_m$ to reach a maximum $Q_m$ value of 115 at $x = 0.03$ as shown in Fig. 11(d). The increased $Q_m$ value could be due to the creation of oxygen vacancies when the lower-valence $Ti^{4+}$ ions replaced the higher-valence $Nb^{5+}$ and $Sb^{5+}$ ions, which improved the "hardness" properties of the BIT-doped KNLNS ceramics and increased the $Q_m$ value to 115 at $x = 0.03$, similar to the study reported by Dong et al. Dong et al. (2017).

Generally, the improved piezoelectric parameters ($k_p$, $d_{33}$, and $Q_m$) may be due to the effect of multiple $Bi^{3+}$ and $Ti^{4+}$ impurities in BIT-doped KNLNS ceramics.

## 4 Conclusions

The BIT templates were fabricated using the molten salt method. The as-synthesized BIT templates exhibited orthorhombic perovskite structures with 5–20 $\mu$m long and 0.5–1 $\mu$m wide plate-like morphologies. At an 1100 °C sintering temperature and a 0.02 mol BIT content, the 0.98KNLNS + 0.02BIT ceramics exhibited a high ceramic density of 4.51 g/cm$^3$ with a fairly uniform microstructure, clear grain boundaries, and a large grain size of 1.29 $\mu$m. The 0.98 KNLNS + 0.02BIT ceramics obtained optimum piezoelectric properties of $k_p = 0.36$, $d_{33} =$ 189 pC/N, $\varepsilon_r = 1017$, $Q_m = 115$, and a high $T_C = 381$°C.

## Acknowledgments

This research is funded by Vietnam National Foundation for Science and Technology Development (NAFOSTED) under grant number 103.02-2023.13.

## References

Chen, Z., Jiang, H., Jin, W., & Shi, C. (2016). Enhanced photocatalytic performance over Bi4Ti3O12 nanosheets with controllable size and exposed 0 0 1 facets for Rhodamine B degradation. *Applied Catalysis B: Environmental*, 180, 698-706.

Dong, Z.J., Pu, Y.P., & Liu, Y.W. (2017). Influence of Bi4Ti3O12 doping on structural and piezoelectric properties of (K0. 4425Na0. 52Li0. 0375)(Nb0. 87Ta0. 06Sb0. 07) O3 lead-free ceramics. *Ceramics International*, 43, S55-S58.

Gio, P.D., Vuong, L.D., & ThanhTung, V. (2021). Phase transition behavior and electrical properties of lead-free (1-x) KNLNS-x BNKZ piezoelectric ceramics. *Journal of Electroceramics, 46*(3), 107-114.

Jiang, C., Tian, X., & Shi, G. (2016, December). K0. 5Na0. 5NbO3 piezoelectric ceramics and its composites fabricated from hydrothermal powders. In 2016 *4th International Conference on Sensors, Mechatronics and Automation* (ICSMA 2016) (pp. 321-327). Atlantis Press.

Li, J., Wang, J., Wu, F., Ma, H., Ma, T., Tian, Y., ... & Yang, B. (2022). Microstructure and electric properties of Bi2O3-doped (K0. 5Na0. 5) NbO3 lead-free ceramics. *Coatings, 12*(4), 526.

Li, Y., Li, L., & Li, B. (2015). Direct ink writing of three-dimensional (K, Na) NbO3-based piezoelectric ceramics. *Materials, 8*(4), 1729-1737.

Long, C., Chang, Q., & Fan, H. (2017). Differences in nature of electrical conductions among Bi4Ti3O12-based ferroelectric polycrystalline ceramics. *Scientific Reports, 7*(1), 4193.

Truong-Tho, N., Le Vuong, D. (2021). Study on the strain behavior and piezoelectric properties of lead-free Bi0. 5 (Na0. 8K0. 2) 0.5 TiO3 ceramics modified with Sn4+ ions. *Journal of Materials Science: Materials in Electronics, 32*(12), 16601-16611.

Tu, L.T.U., Vuong, L.D., Dat, T.N., & Tung, V.T. (2025). Effects of CuO doping on the sintering behavior and piezoelectric properties of lead-free (K0. 41Na0. 59)(Nb0. 84Sb0. 06Ta0. 10) O3 ceramics. *Applied Physics A, 131*(3), 210.

Tu, L.T.U., Vuong, L.D., Cuong, N.X., Lich, N.Q., Nhat, N.D., Hieu, L.D., ... & Wei, P.C. (2024a). Improvement of the electrical properties of textured BNKT-modified (K, Na) NbO3 lead-free ceramics in the broad operating temperature range. *Journal of Materials Science: Materials in Electronics, 35*(19), 1363.

Tu, L.T.U., Vuong, L.D. (2024b). Utilizing TiO2 nanostructures to synthesize plate-like Bi4Ti3O12 templates via molten salt method. *Eurasian Journal of Physics and Functional Materials, 8*(2), 84-92.

Tu, L.T.U., Tho, N.T. (2023). Selection and optimization of Sb and Ta co-doped (K0. 41Na0. 59)(Nb1-x-ySbxTay) O3 lead-free ceramics. *Journal of Materials Science: Materials in Electronics, 34*(10), 917.

Ullah, A., Ahn, C.W., Hussain, A., & Kim, I.W. (2010). The effects of sintering temperatures on dielectric, ferroelectric and electric field-induced strain of lead-free Bi0. 5 (Na0. 78K0. 22) 0.5 TiO3 piezoelectric ceramics synthesized by the sol–gel technique. *Current Applied Physics, 10*(6), 1367-1371.

Vuong, L.D., Tho, N.T. (2017). The sintering behavior and physical properties of Li2CO3-doped Bi0. 5 (Na0. 8K0. 2) 0.5 TiO3 lead-free ceramics. *International Journal of Materials Research, 108*(3), 222-227.

Vuong, L.D., Cuong, N.X., Lich, N.Q., Nhat, N.D., Hieu, L.D., Nha, V.Q., ... & Dat, T.N. (2025). The effect of BaZrO3 content on the structure, microstructure, and electrical properties of (K, Na) NbO3-based lead-free ceramics. *Applied Physics A, 131*(5), 383.

Vuong, L.D., Lich, N.Q., Cuong, N.X., Nha, V.Q., Nhat, N.D., Hieu, L.D., Son, L.P., ... & Wei, P.C. (2023). Optimization of the calcination and two-step sintering temperatures of (K0. 48Na0. 48Li0. 04)(Nb0. 95Sb0. 05) O3 ceramics. *Materials Research Express, 10*(10), 105701.

Wang, Y., Lu, Y., Wu, M., Wang, D., Li, Y., & Wang, Y. (2012). Phase Structure and Enhanced Piezoelectric Properties of Lead-Free Ceramics $(1 - x)(K_{0.48}Na_{0.52})NbO_3$–$(x/5.15)K_{2.9}Li_{1.95}Nb_{5.15}O_{15.3}$ with High Curie Temperature. *International Journal of Applied Ceramic Technology, 9*(1), 221-227.

Wang, L., Ma, W., Fang, Y., Zhang, Y., Jia, M., Li, R., & Huang, Y. (2013). Bi4Ti3O12 synthesized by high temperature solid phase method and it's visible catalytic activity. *Procedia Environmental Sciences,* 18, 547-558.

Wei, D.D., Yuan, Q.B., Zhang, G.Q., & Wang, H. (2015). Templated grain growth and piezoelectric properties of¡ 001¿-textured PIN–PMN–PT ceramics. *Journal of Materials Research, 30*(14), 2144-2150.

Wendari, T.P., Ikhram, M. (2022). Compositional-induced structural transformation and relaxor ferroelectric behavior in Sr/Nb-modified Bi4Ti3O12 Aurivillius ceramics. *Ceramics International, 48*(20), 30598-30605.

Xie, Z., Tang, X., Shi, J., Wang, Y., Yuan, G., & Liu, J. M. (2022). Excellent piezo-photocatalytic performance of Bi4Ti3O12 nanoplates synthesized by molten-salt method. *Nano Energy,* 98, 107247.

Zhang, Y., Wang, S., Chen, C., Zhang, N., Wang, A., Zhu, Y., & Cai, F. (2018). Enhanced linearity of KNNS-BNKZ ceramics by combining the controls of phase composition and microstructure. *Ceramics International, 44*(7), 8380-8386.

Zhao, L., Zhang, B.P., Zhou, P.F., Zhao, X.K., & Zhu, L.F. (2014). Phase structure and property evaluation of (Ba, Ca)(Ti, Sn) O 3 sintered with Li 2 CO 3 addition at low temperature. *Journal of the American Ceramic Society, 97*(7), 2164-2169.